ELSEVIER

Contents lists available at ScienceDirect

# Next Nanotechnology

journal homepage: www.sciencedirect.com/journal/next-nanotechnology





# Au nanopillar array prepared by selective etching of Au-Sr<sub>3</sub>Al<sub>2</sub>O<sub>6</sub> vertically aligned nanocomposite thin films

Benson Kunhung Tsai <sup>a</sup>, Jiawei Song <sup>a</sup>, Juncheng Liu <sup>a</sup>, Jianan Shen <sup>a</sup>, Yizhi Zhang <sup>a</sup>, Xinghang Zhang <sup>a</sup>, Haiyan Wang <sup>a,b,\*</sup>

- <sup>a</sup> School of Materials Engineering, Purdue University, West Lafayette, IN 47907, United States
- <sup>b</sup> School of Electrical and Computer Engineering, Purdue University, West Lafayette, IN 47907, United States

#### ARTICLE INFO

Keywords:
Vertically aligned nanocomposite
Au nanopillars
Selective etching
Plasmonic resonance
Hyperbolic properties

#### ABSTRACT

Au nanostructures offer a wide range of applications such as surface-enhanced Raman spectroscopy, photovoltaics, and biosensors. Effective integrating well-controlled Au nanostructures on chip via a self-assembly process remains challenging as most of the Au nanostructures were prepared by either chemical synthesis methods or lithography patterning techniques. This study introduces a simple two-step approach for fabricating Au nanostructures on substrate with well controlled morphology and density. First, epitaxial Au-Sr<sub>3</sub>Al<sub>2</sub>O<sub>6</sub> (SAO) vertically aligned nanocomposites (VANs) were deposited on SrTiO<sub>3</sub> substrates. Second, by subsequently dissolving the water-soluble SAO matrix, various Au nanostructures ranging from 0D nanoparticles to 1D nanopillars are demonstrated. The Au morphology tuning is achieved by varying the deposition parameters of the VANs. This method eliminates the need of harsh chemical solutions and tedious lithography/patterning steps. These findings provide a novel strategy for tailoring the Au nanostructures and their optical properties, and, demonstrating on-chip integration for advanced optical device applications.

# Introduction

The pioneering demonstration of gold (Au) nanoparticles by wet chemistry methods marked a significant milestone in nanomaterial research [1]. Since then versatile chemical methods have been employed to synthesize diverse shapes of Au nanomaterials [2–5]. One of the fascinating physical properties of the Au nanomaterial compared to its bulk counterpart is its unique optical properties. For example, local surface plasmon resonance for Au nanostructures is a unique property that the free electrons on the surface start to oscillate, when the external light source illuminates on nanostructured Au at a specific frequency [2, 6]. Interestingly, 1D nanostructures could result in two distinct plasmonic responses: the longitude mode and transverse mode due to the structural anisotropy nature. These different modes cause the electron to oscillate in different light frequencies, one in the near-infrared region and the other in the visible region [6]. Such tunable plasmonic responses offer numerous opportunities for applications in surface-enhanced spectroscopy, photocatalysis, photothermal therapy, etc [2,6,7].

Various synthesis methods have been utilized to obtain Au nanostructures in 1D structure. One common approach involves the use of wet chemistry methods with surfactants and Ag catalyst to break the symmetry of Au nanoparticles [8]. However, this method often generates chemical waste [9]. Moreover, the presence of precursor element, such as the Ag atoms, can remain in the final product of Au nanowires [8,10]. Another commonly used method is the deposition of Au into the pores of anodic aluminum oxide (AAO) membranes [11,12]. Since the pore of AAO is predefined, the diameter of the Au nanostructures on the transverse side becomes limited.

As an alternative approach, oxide-metal based vertically aligned nanocomposite (VAN) structure offers an intriguing technique for synthesizing uniform and high-density Au nanopillars [13,14]. In the VAN structure, one phase is embedded as nanopillars or nanodomains within a matrix material. Zhang *et al.* demonstrated that by tuning the thickness of the thin film, Au can be formed in various shapes ranging from nanoparticles to nanopillars, thereby enabling to tune optical responses [15]. Additionally, the incorporation of different matrix materials in the VAN structure provides the opportunity for additional functionalities such as ferromagnetic [16], ferroelectric [17], and others [13]. In general, these oxide-metal VANs present a 3D structure with metal nanopillars embedded in oxide matrix with unique electrical, optical, and

<sup>\*</sup> Corresponding author at: School of Materials Engineering, Purdue University, West Lafayette, IN 47907, United States. E-mail address: hwang00@purdue.edu (H. Wang).

magnetic properties. Such freestanding 1D Au nanostructures without the oxide matrix remains challenging.

In this study, we present a novel approach for the synthesis of freestanding 1D Au nanopillars based on water-dissolvable VANs deposited by pulsed laser deposition (PLD). A water-soluble oxide, Sr<sub>3</sub>Al<sub>2</sub>O<sub>6</sub> (SAO), was adopted as the matrix material to embed the Au nanopillars to form a tailorable VAN structure. SAO has recently been employed as a sacrificial buffer layer for processing free-standing oxide thin films and oxide film transfer. [18-22] Because of no strain effect from the substrate, these freestanding materials exhibit unexpected phenomena, such as unexpected polarization in ultrathin thickness [23], super-elastic property of oxides [24], and induced ferroelectric property from non-ferroelectric material [25]. As shown in the schematic drawings in Fig. 1, a simple two-step approach (i.e., (a) and (b) steps) has been proposed for fabricating Au nanostructures on substrate with well controlled morphology and density. First, in step a, epitaxial Au-SAO vertically aligned nanocomposites (VANs) were deposited on SrTiO<sub>3</sub> (STO) substrates. Second, in step b, by subsequently dissolving the water-soluble SAO matrix, various Au nanostructures ranging from 0D nanoparticles to 1D nanopillars are demonstrated. The Au morphology tuning is achieved by varying the deposition parameters of the VANs, which is confirmed by transmission electron microscopy (TEM), scanning transmission electron microscopy (STEM) and EDX mapping. The tunable optical properties before and after water etching were characterized and compared by UV-vis transmittance and ellipsometry measurements. This simple method of integrating 1D Au nanostructures on chip can be directly adopted by future optical device fabrications without harsh chemicals and multi-step lithography patterning process.

# **Experimental section**

# Composite thin film growth

The  $Sr_3Al_2O_6$  (SAO) target was prepared by mixing  $SrCO_3$  and  $Al_2O_3$  powders in their stoichiometric ratio. The resulting powder mixture was then subjected to a sintered process at  $1300~^{\circ}C$ . Then, an Au strip was attached to the SAO target by silver paste to serve as the composite

target. All films were deposited on to  $SrTiO_3$  (001) single crystal substrates (MTI Corporation) and at 800 °C.  $O_2$  pressure of 50–200 mTorr, laser repetition rate of 2–10 Hz, and different laser energy were selected to obtain different Au nanostructures SAO-Au thin film. After growth, the thin films were cooled under the rate of 10 °C/min.

# Characterization of the thin film nanostructure

All  $2\Theta$ - $\omega$  X-ray diffraction scans were performed with a PANalytical Empyrean diffractometer to identify the crystallinity of the SAO and Au. All samples for TEM were prepared by mechanically grinding and dimpling, followed by subsequent argon-ion milling using a Gatan Precision Ion milling system for the final polish. All TEM experiments were carried out using a Thermo Fisher Scientific TALOS 200X TEM operated at 200 kV.

#### Results and discussion

First, self-assembled SAO-Au VAN nanocomposites were initially deposited onto the STO substrates. The STO (a=3.905 Å) substrate was selected due to its close lattice matching with Au (a=4.080 Å) and SAO (a=15.844 Å, a/4=3.961 Å), which could facilitate the epitaxial growth of VAN nanostructures [26]. The schematic illustration on the final nanostructure of the thin film is shown in Fig. 1a. Such structure is obtained by a self-assembled method [17,27]. By controlling the laser frequencies in the range of 2 Hz to 10 Hz, different Au morphologies were successfully obtained, which is to be discussed later. Fig. 1b shows the Au nanopillars after water vapor etching. We adopted a new etching method as previously mentioned by others [28], i.e., water vapor etching, instead of the direct water etching, to avoid the detachment of the Au nanopillars from the substrates.

# Nanostructure analysis

Following the depositions, a comprehensive microstructural analysis was conducted. Full  $\theta$ -2 $\theta$  scans of XRD were carried out in the range of  $10^{\circ}$ - $90^{\circ}$  as shown in Fig. 2. Fig. 2a compares the XRD plots for samples

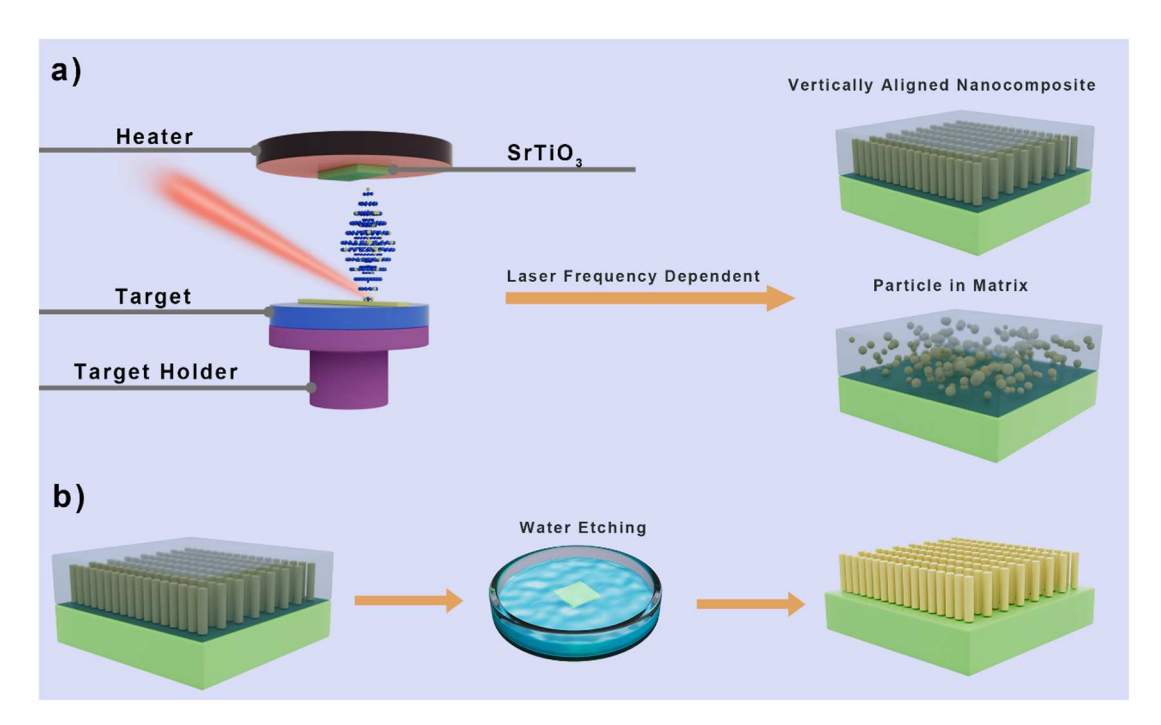


Fig. 1. Schematic illustration of the SAO-Au nanocomposite deposition and water etching process.a) Au nanopillars embedded within SAO matrix. The thin films were deposited under laser frequencies of either 2 Hz or 5 Hz. b) Au nanoparticles embedded within SAO matrix deposited under laser frequency of 10 Hz. c) etching process to obtain the Au nanopillars.

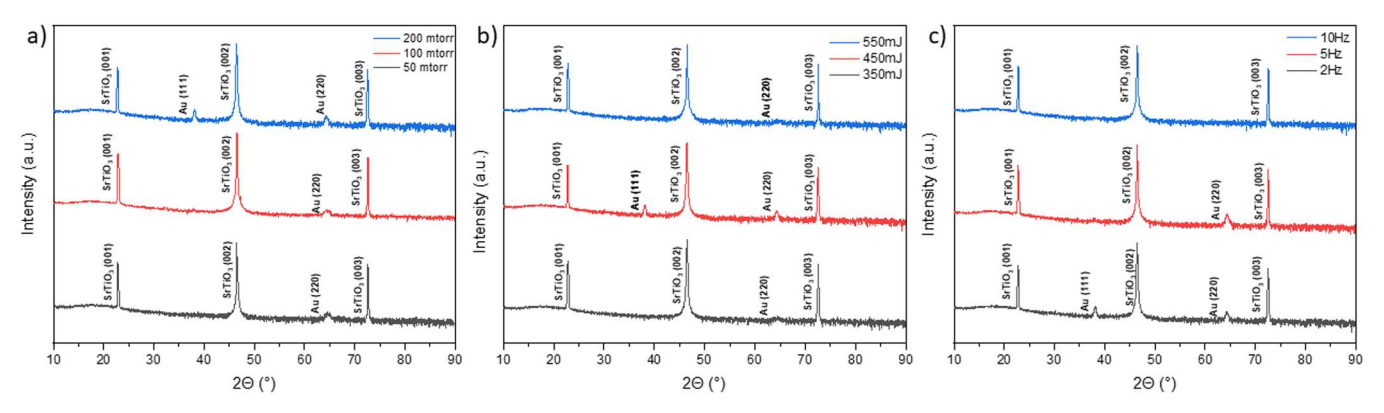


Fig. 2. Microstructure analysis by XRD. SAO-Au nanocomposite thin films were synthesized under different conditions. Samples were synthesize under a) different oxygen partial pressure b) different laser energy and c) different laser frequencies.

prepared under different oxygen partial pressures, and Fig. 2b illustrates the results for samples deposited under different laser energy. The Au (220) peak is consistently observed in all the samples regardless of their processing conditions, while the Au (111) peak only appears in the cases of the sample deposited under 450 mJ laser energy, and the sample deposited under 200 mTorr oxygen pressure. The appearance of the Au (111) peak potentially indicates the formation of a 1D nanopillar [15]. Such a result is consistent for the 2 Hz sample. However, the nanopillar forms without showing the Au (111) peak for the 5 Hz sample.

The SAO (002) peak is not very apparent in the XRD plots. A detailed XRD scan was thus performed near the STO (002) to observe the SAO peak and is shown in Figure S1a. The detailed scan doesn't show a SAO peak, since the lattice parameter of SAO (a=15.844 Å, a/4=3.961 Å) is very close to that of the STO and the SAO peak intensity might be low. It could also be explained by the growth mechanism of the VAN. The

growth mechanism of the VAN can be explained by the strain mechanism, which has been reported previously. It is critical to have the correct in-plane strain between the nanocomposite thin film and the substrate. Most oxide-metal based VANs show that the oxide material has a larger lattice parameter than the substrate material, but the metal has a smaller lattice parameter than the substrate material. Here, the lattice parameter for Au is 4.08 Å, and for SAO, it is 15.844 Å (a/4=3.961 Å). This indicates that the strain coupling between the SAO and Au makes it difficult to form an epitaxial oxide-metal VAN on the STO substrate. The enlarged XRD in Figure S1a and the selected area electron diffraction (SAED) pattern in Figure S1b shows textured SAO on the STO substrate. Fig. 2c displays the XRD plot obtained for samples with tuning the laser frequency. Notably, as the laser frequency decreases, both the Au (220) and Au (111) peaks are both observed for the sample deposited under the lowest laser frequency (2 Hz). As the laser frequency

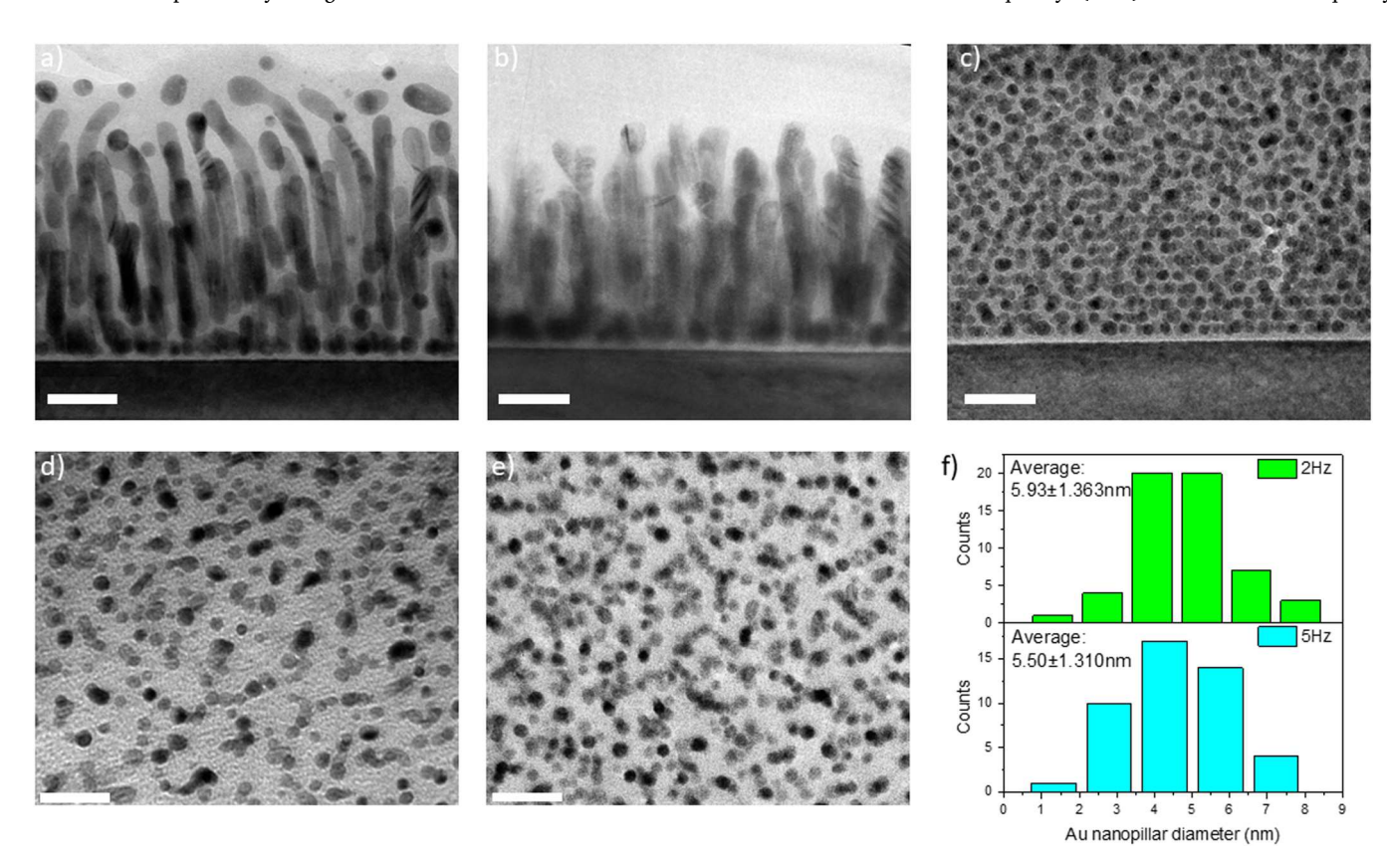


Fig. 3. The TEM images of SAO-Au VANs deposited under different laser frequencies. Cross-sectional TEM images of the samples deposited under a) 2 Hz, b) 5 Hz and c) 10 Hz. Plan-view TEM images of the d) 2 Hz and e) 5 Hz samples; f) Histograms of the diameter of the Au nanopillars in 2 Hz and 5 Hz samples suggesting that the average diameter of the nanopillars in the 2 Hz sample (5.93 nm) is slightly larger than that of the 5 Hz sample (5.50 nm). All scale bars are 20 nm.

increases, the Au (111) peak disappears, and eventually all Au peaks vanish completely for 10 Hz deposition. This diffraction pattern variation suggests a potential change in the morphology of the Au nanostructures, which leads to a further detailed nanostructure analysis through transmission electron microscopy (TEM).

After XRD analysis, a detailed nanostructure analysis using TEM was conducted to further investigate the morphology and structure of the SAO-Au VAN thin films deposited with various laser frequencies. Crosssectional TEM images of the films are presented in Fig. 3a-c, revealing distinct Au morphologies. With lower laser frequencies (i.e., 2 Hz and 5 Hz) in Fig. 3a and b, respectively, the Au nanostructures shows in nanopillar form, while the highest frequency deposition (i.e., 10 Hz) results in Au nanoparticles in Fig. 3c. The corresponding cross-sectional EDS mapping result in Figure S1 confirms the presence of the Au nanostructures embedded within the SAO matrix. To further explore the nanopillar density and distribution, plan-view TEM imaging was performed for the 2 Hz and 5 Hz samples. Fig. 3d and e display the planview TEM images of the samples grown under the laser frequencies of 2 Hz and 5 Hz, respectively. The images reveal the uniform distribution of the Au nanopillars in both samples with more detailed particle size distribution analysis shown in the histogram plots in Fig. 3f. Additional elemental analysis by STEM-EDS is present in Figure S2. The TEM, STEM and STEM-EDS results provide conclusive evidence of the VAN nanostructures with different Au morphologies. It is clear that the average diameter of the nanopillars in the 2 Hz sample (d=5.93 nm) is slightly larger than that of the 5 Hz sample (d=5.50 nm), while the density of pillars in the 2 Hz sample is lower than that of the 5 Hz sample. This is attributed to the adatom diffusion process during deposition. Lower laser frequencies will result in longer diffusion time between the laser

pulses and lower adatom density, thus result in larger pillar diameters and lower pillar densities, compared to those of the higher laser frequencies. Previous studies have also investigated the effect of laser frequency on the VAN structure [29]. The results here are consistent with prior reports. Notably, the 10 Hz deposition showed Au nano-structure in the form of nanoparticles, indicating insufficient nucleation time for the Au adatoms to form nanopillar structures.

An important property of the VAN structure with Au nanopillar embedded in various dielectric matrix materials is its strong optical anisotropy [15]. To investigate optical anisotropy, ellipsometry analysis was conducted for the SAO-Au thin films synthesized under different laser frequencies -in the wavelength range of 400-2000 nm. The ellipsometric  $\Psi$  and  $\Delta$  data were then fitted using the B-spline model coupled with the uniaxial model, allowing us to obtain the optical permittivity, as shown in Fig. 4a. The fitted data provides the real and imaginary parts of the in-plane  $(\varepsilon_{\parallel})$  and out-of-plane  $(\varepsilon_{\perp})$  permittivity. The real part of the permittivity  $(\varepsilon')$  for the in-plane  $(\parallel)$  and out-of-plane direction  $(\perp)$ as a function of wavelength is plotted in Fig. 4a.  $\varepsilon_{\parallel}^{'}$  in Fig. 4a shows positive values across the entire wavelength range. For the  $\perp$  direction, 2 and 5 Hz samples show a similar behavior across the wavelength range, i.e., the  $\varepsilon_{\perp}^{'}$  transition from positive values to negative values for 2 Hz and 5 Hz. Based on this observation, the 2 Hz and 5 Hz samples exhibit obvious optical anisotropy with a Type I hyperbolic behavior as illustrated in Fig. 4b. It is noted that the epsilon near zero (ENZ) value is different for the two cases, i.e., 725 nm for the 2 Hz sample and 750 nm for the 5 Hz one. Such wavelength where the permittivity value shifts from positive to negative is known as the ENZ resonance wavelength [14]. To further illustrate the optical anisotropy property based on the

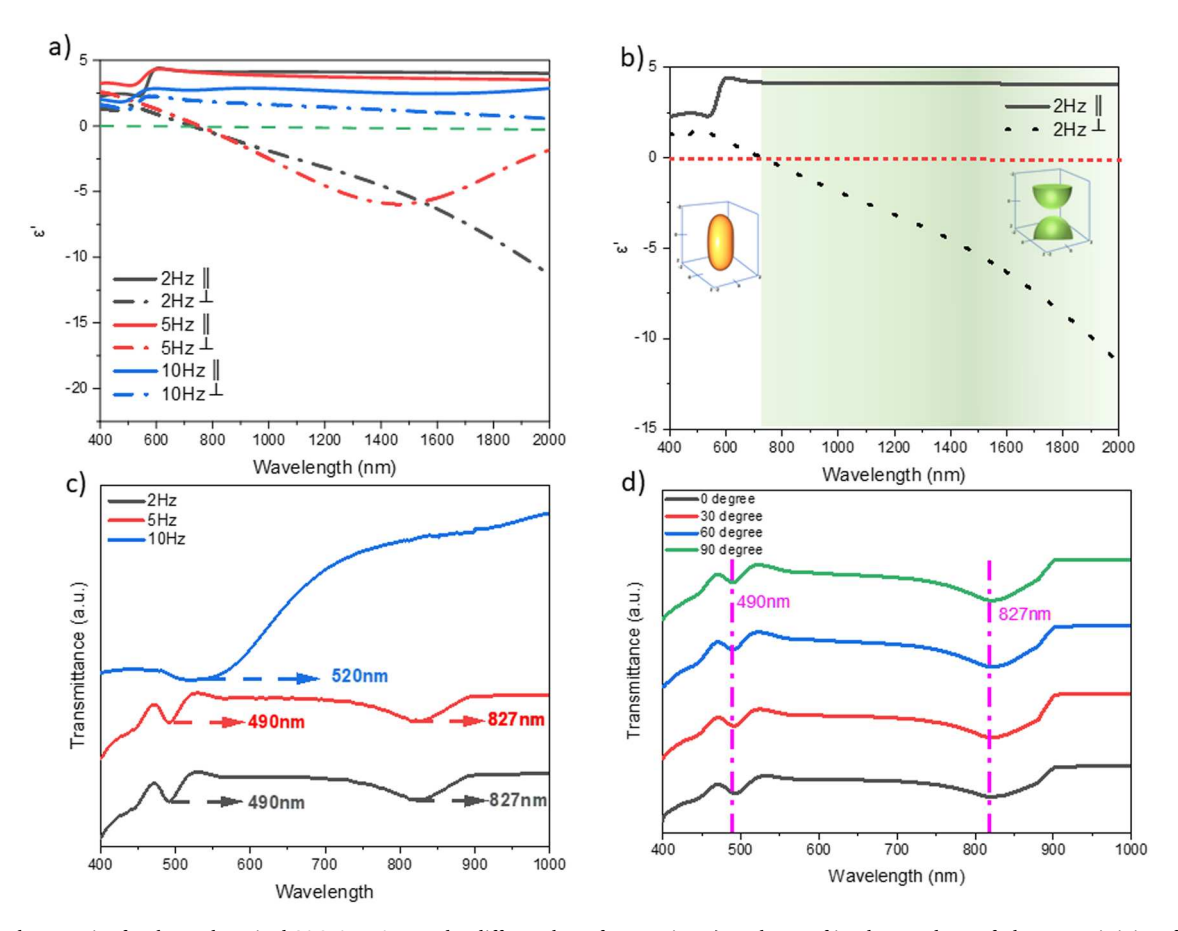


Fig. 4. Optical properties for the as-deposited SAO-Au VANs under different laser frequencies. a) Real part of in-plane and out-of-plane permittivity of the SAO-Au nanocomposites; b) enlarged figure for the 2 Hz sample to illustrate the hyperbolic region beyond 725 nm. c) Optical transmittance spectra in Vis-NIR region for films that deposited under different laser frequencies under direct incidence. d) angular dependent transmittance test, which shows that the plasmonic responses are in the visible and NIR region.

optical permittivity, the permittivity of the 2 Hz sample is individually plot in Fig. 4b, with an inset of isofrequency surface topology similar to prior reports [15,17]. When the wavelength of 725 nm is exposed onto the thin film, the isofrequency of the thin film becomes hyperbola, which is known as hyperbolic dispersion. This behavior indicates that the thin film behaves like a metal in the vertical direction and a dielectric in parallel, resulting in optical anisotropy [15,30].

To further investigate the optical properties of the SAO-Au VAN structure, the optical transmittance measurement and angulardependent transmittance measurement were performed to determine the localized surface plasmon resonance (LSPR) position for the Au nanopillar. The transmittance result of all the films measured at  $0^{\circ}$  is shown in Fig. 4c. Different nanostructures exhibit distinct plasmonic responses. The nanoparticle sample (deposited under 10 Hz) only shows the plasmonic response at 520 nm. An interesting dual plasmonic response (at the wavelengths of 490 nm and 827 nm) is observed in the 2 Hz and 5 Hz samples, which has not been widely reported in previous oxide-metal VAN structure. The two plasmonic responses observed in the nanopillar samples could be attributed to the different plasmonic response from the transverse side and the longitudinal side of the nanopillars, similar to previous reported anisotropic Au nanostructures [2,6]. It is noted that some of the Au nanopillars did not grow perfectly straight as shown in Figure S1, which leads to the exposure of the longitudinal side of the Au nanopillars. Changing the size of the nanoparticle and nanowire will result in a peak shift [2]. By tilting the angle of the sample, the amount of surface area that is exposed to the light increases. An angular-dependent transmittance test within the angle range of 0°-90° has been performed. Figure S4a shows a schematic illustration of the angle defined in the measurements. Figure S4b shows that the peak positions of the plasmonic responses for the VAN structure remain unchanged. This might be due to the morphology variation of Au nanopillars. According to the STEM image in Figure S2a, it shows that there are length and diameter variations in the Au nanopillars. Since the plasmonic response depends on the average length of the nanopillars, upon sample tilting, the average surface area of the Au nanopillars exposed did not change significantly and the overall plasmonic peak position did not vary [31].

Lastly, the optical responses of the samples after etching the SAO matrix have also being measured. Direct water etching of the SAO-Au nanocomposite sample causes that Au nanopillars were detached from the substrate. Since the humidity can affect the quality of SAO as previously reported [26], we thus used the water vapor to control the humidity to partially etch the SAO matrix. This method is schematically illustrated in Figure S5. The relative humidity has been controlled at around 70 %, where it enables us to regulate the amount of water vapor used for etching the SAO matrix. As an example, a 2 Hz sample has been selected and etched. The resulting plasmonic response with time-dependent etching was investigated under 90°, which is shown in Figure S7a. The result shows the plasmonic responses in visible region and near-infrared region are still shown, but with much weaker signal than that of the as-deposited samples. The weaker signal could be related to the smaller amount of Au nanostructures on the substrate. Since the Au is not attached to the substrate, the Au nanowire can detach from the substrate after 12 hours of etching as shown in Figure S7b. Such a removal process of the Au nanowire from the substrate could result in a weaker signal. The scanning electron microscopy (SEM) image in Figure S8 depicts the sample before etching and after 12 hours of etching, providing visual evidence of the etching process.

This work demonstrates the feasibility of the direct growth of SAO-Au VAN, incorporating a water-etchable oxide SAO as the matrix for the preparation of various Au nanostructures. This novel approach involves the use of different laser frequencies to tune the Au geometry, thereby avoiding the need for any chemical precursors, which makes the process more environmentally friendly and simpler, compared to the previous demonstrated chemical-based synthesis methods [23]. In addition, by manipulating Au nanostructures, it shows specific optical

responses that span from the visible to near-infrared wavelength. Such interesting optical property and synthesis technique provides a new choice of material for future applications in optical-based chemical sensors and nanoscale optical devices. Further work is needed to enhance the adhesion between the substrate and the Au nanopillars. Other metals beyond Au demonstrated in this work can also be considered in the future for achieving the well-dispersed metal nanostructures, such as Co, Fe and Ni magnetic nanostructures. These unique metallic nanostructures prepared via the water-etchable oxide-metal VANs can find various applications in catalysis, optical sensors, integrated photonics, magnetic sensors and spintronic devices.

# Conclusion

This study presents a new and alternative method for synthesizing controlled Au nanopillar structures using the SAO-Au VAN structures followed by water etching of the SAO matrix. Tunable Au nanostructures varied from nanopillars to nanoparticles have been demonstrated by tuning the deposition frequency. The unique optical anisotropy of the SAO-Au VAN structure, and the observation of two distinct plasmonic responses have been observed in the 2 Hz and 5 Hz samples with clear Au nanopillar structures. This demonstration presents great potential of integrating Au nanopillars and other Au nanostructures on chip using the direct deposition of SAO-Au nanocomposite followed by the water vapor etching method. This method could find a wide range of applications, such as optical sensors and plasmonic photonic nanostructures and devices.

# CRediT authorship contribution statement

B.K.T. and H.W.: Conceptualization, Methodology, Investigation, Formal analysis, Validation, Visualization, Writing-Original Draft. B.K. T., J.S., J.L. J.S., Y.Z. and H.W.: Nanostructure characterization, Formal analysis, Writing-review & editing. B.K.T., J.S. Optical property characterization. X.Z. and H.W.: Conceptualization, Methodology, Writing-review & editing, Project administration, Funding acquisition, Supervision, Resources.

# **Declaration of Competing Interest**

The authors declare that they have no known competing financial interests or personal relationships that could have appeared to influence the work reported in this paper.

# Acknowledgements

This work is supported by the U.S. National Science Foundation (DMREF-2323752). J.L. and H.W. aknowledge the support from the U.S. Department of Energy, Office of Science, Basic Energy Sciences under Award DE-SC0020077 for the optical measurements. J.S., Y.Z. and H.W. acknowledge the support from the U.S. National Science Foundation for the microscopy analysis (DMR-2016453). This paper describes objective technical results and analysis. Any subjective views or opinions that might be expressed in the paper do not necessarily represent the views of the U.S. Department of Energy or the United States Government.

# Appendix A. Supporting information

Supplementary data associated with this article can be found in the online version at doi:10.1016/j.nxnano.2024.100071.

#### References

 J. Turkevich, P.C. Stevenson, J. Hillier, A study of the nucleation and growth processes in the synthesis of colloidal gold, Discuss. Faraday Soc. 11 (0)) (1951) 55–75.

- [2] X. Yang, M. Yang, B. Pang, M. Vara, Y. Xia, Gold nanomaterials at work in biomedicine, Chem. Rev. 115 (19) (2015) 10410–10488.
- [3] H.B. Jeon, P.V. Tsalu, J.W. Ha, Shape effect on the refractive index sensitivity at localized surface plasmon resonance inflection points of single gold nanocubes with vertices, Sci. Rep. 9 (1) (2019) 13635.
- [4] N.R. Jana, L. Gearheart, C.J. Murphy, Seeding growth for size control of 5–40 nm diameter gold nanoparticles, Langmuir 17 (22) (2001) 6782–6786.
- [5] Y. Yang, J. Liu, Z.-W. Fu, D. Qin, Galvanic replacement-free deposition of Au on Ag for core-shell nanocubes with enhanced chemical stability and SERS activity, J. Am. Chem. Soc. 136 (23) (2014) 8153–8156.
- [6] J. Zheng, X. Cheng, H. Zhang, X. Bai, R. Ai, L. Shao, J. Wang, Gold nanorods: the most versatile plasmonic nanoparticles, Chem. Rev. 121 (21) (2021) 13342–13453.
- [7] Y.H. Jang, Y.J. Jang, S. Kim, L.N. Quan, K. Chung, D.H. Kim, Plasmonic solar cells: from rational design to mechanism overview, Chem. Rev. 116 (24) (2016) 14982–15034.
- [8] M.J. Walsh, S.J. Barrow, W. Tong, A.M. Funston, J. Etheridge, Symmetry breaking and silver in gold nanorod growth, ACS Nano 9 (1) (2015) 715–724.
- [9] S. Balasubramanian, A. Sheelam, K. Ramanujam, R. Dhamodharan, Green, seed-mediated synthesis of Au nanowires and their efficient electrocatalytic activity in oxygen reduction reaction, ACS Appl. Mater. Interfaces 9 (34) (2017) 20202.
- [10] S.R. Jackson, J.R. McBride, S.J. Rosenthal, D.W. Wright, Where's the silver? Imaging trace silver coverage on the surface of gold nanorods, J. Am. Chem. Soc. 136 (14) (2014) 5261–5263.
- [11] S.R. Nicewarner-Peña, R.G. Freeman, B.D. Reiss, L. He, D.J. Peña, I.D. Walton, R. Cromer, C.D. Keating, M.J. Natan, Submicrometer metallic barcodes, Science 294 (5540)) (2001) 137–141.
- [12] K. Kim, X. Xu, J. Guo, D.L. Fan, Ultrahigh-speed rotating nanoelectromechanical system devices assembled from nanoscale building blocks, Nat. Commun. 5 (1) (2014) 3632.
- [13] S. Misra, L. Li, D. Zhang, J. Jian, Z. Qi, M. Fan, H.-T. Chen, X. Zhang, H. Wang, Self-assembled ordered three-phase Au–BaTiO3–ZnO vertically aligned nanocomposites achieved by a templating method 31 (7)) (2019) 1806529.
- [14] D. Zhang, S. Misra, L. Li, X. Wang, J. Jian, P. Lu, X. Gao, X. Sun, Z. Qi, M. Kalaswad, X. Zhang, H. Wang, Tunable optical properties in self-assembled oxide-metal hybrid thin films via Au-phase geometry control: from nanopillars to nanodisks, Adv. Opt. Mater. 8 (4) (2020) 1901359.
- [15] D. Zhang, S. Misra, L. Li, X. Wang, J. Jian, P. Lu, X. Gao, X. Sun, Z. Qi, M. Kalaswad, X. Zhang, H. Wang, Tunable optical properties in self-assembled oxide-metal hybrid thin films via Au-phase geometry control: from nanopillars to nanodisks 8 (4)) (2020) 1901359.
- [16] J. Lu, R.L. Paldi, Y. Pachaury, D. Zhang, H. Wang, M. Kalaswad, X. Sun, J. Liu, X. L. Phuah, X. Zhang, A.A. El-Azab, H. Wang, Ordered hybrid metamaterial of La0.7Sr0.3MnO3–Au vertically aligned nanocomposites achieved on templated SrTiO3 substrate, Mater. Today Nano 15 (2021) 100121.
- [17] J. Liu, X. Wang, X. Gao, H. Wang, J. Jian, J. Huang, X. Sun, Z. Qi, S. Misra, Z. He, H. Wang, Multifunctional self-assembled BaTiO3-Au nanocomposite thin films on flexible mica substrates with tunable optical properties, Appl. Mater. Today 21 (2020) 100856.

- [18] P. Su, H. Wen, Y. Zhang, C. Tan, X. Zhong, Y. Wu, H. Song, Y. Zhou, Y. Li, M. Liu, J. Wang, Super-flexibility in freestanding single-crystal SrRuO3 conductive oxide membranes, ACS Appl. Electron. Mater. 4 (6) (2022) 2987–2992.
- [19] G. Dong, S. Li, T. Li, H. Wu, T. Nan, X. Wang, H. Liu, Y. Cheng, Y. Zhou, W. Qu, Y. Zhao, B. Peng, Z. Wang, Z. Hu, Z. Luo, W. Ren, S.J. Pennycook, J. Li, J. Sun, Z.-G. Ye, Z. Jiang, Z. Zhou, X. Ding, T. Min, M. Liu, Periodic wrinkle-patterned single-crystalline ferroelectric oxide membranes with enhanced piezoelectricity, Adv. Mater. 32 (50) (2020) 2004477.
- [20] J. Shen, Z. Dong, M. Qi, Y. Zhang, C. Zhu, Z. Wu, D. Li, Observation of moiré patterns in twisted stacks of bilayer perovskite oxide nanomembranes with various lattice symmetries, ACS Appl. Mater. Interfaces 14 (44) (2022) 50386–50392.
- [21] Xu, R.; Crust, K.J.; Harbola, V.; Arras, R.; Patel, K.Y.; Prosandeev, S.; Cao, H.; Shao, Y.-T.; Behera, P.; Caretta, L.; Kim, W.J.; Khandelwal, A.; Acharya, M.; Wang, M.M.; Liu, Y.; Barnard, E.S.; Raja, A.; Martin, L.W.; Gu, X.W.; Zhou, H.; Ramesh, R.; Muller, D.A.; Bellaiche, L.; Hwang, H.Y., Size-Induced Ferroelectricity in Antiferroelectric Oxide Membranes. n/a (n/a), 2210562.
- [22] J. Shen, B.K. Tsai, K. Xu, A. Shang, J.P. Barnard, Y. Zhang, R. Tripathi, Z. Chen, X. Zhang, H. Wang, A generalized synthesis method for freestanding multiferroic two-dimensional layered supercell oxide films via a sacrificial buffer layer, Nano Res. (2023).
- [23] D. Ji, S. Cai, T.R. Paudel, H. Sun, C. Zhang, L. Han, Y. Wei, Y. Zang, M. Gu, Y. Zhang, W. Gao, H. Huyan, W. Guo, D. Wu, Z. Gu, E.Y. Tsymbal, P. Wang, Y. Nie, X. Pan, Freestanding crystalline oxide perovskites down to the monolayer limit, Nature 570 (7759)) (2019) 87–90.
- [24] G. Dong, S. Li, M. Yao, Z. Zhou, Y.-Q. Zhang, X. Han, Z. Luo, J. Yao, B. Peng, Z. Hu, H. Huang, T. Jia, J. Li, W. Ren, Z.-G. Ye, X. Ding, J. Sun, C.-W. Nan, L.-Q. Chen, J. Li, M. Liu, Super-elastic ferroelectric single-crystal membrane with continuous electric dipole rotation, Science 366 (6464)) (2019) 475–479.
- [25] R. Xu, J. Huang, E.S. Barnard, S.S. Hong, P. Singh, E.K. Wong, T. Jansen, V. Harbola, J. Xiao, B.Y. Wang, S. Crossley, D. Lu, S. Liu, H.Y. Hwang, Straininduced room-temperature ferroelectricity in SrTiO3 membranes, Nat. Commun. 11 (1) (2020) 3141.
- [26] D. Lu, D.J. Baek, S.S. Hong, L.F. Kourkoutis, Y. Hikita, Harold Y. Hwang, Synthesis of freestanding single-crystal perovskite films and heterostructures by etching of sacrificial water-soluble layers, Nat. Mater. 15 (12) (2016) 1255–1260.
- [27] L. Li, L. Sun, J.S. Gomez-Diaz, N.L. Hogan, P. Lu, F. Khatkhatay, W. Zhang, J. Jian, J. Huang, Q. Su, M. Fan, C. Jacob, J. Li, X. Zhang, Q. Jia, M. Sheldon, A. Alù, X. Li, H. Wang, Self-assembled epitaxial Au-oxide vertically aligned nanocomposites for nanoscale metamaterials, Nano Lett. 16 (6) (2016) 3936–3943.
- [28] Y.S. Kim, J. Song, C. Hwang, X. Wang, H. Wang, J.L. MacManus-Driscoll, H.-K. Song, S. Cho, Nanoporous films and nanostructure arrays created by selective dissolution of water-soluble materials. Adv. Sci. 5 (11) (2018) 1800851.
- [29] A. Chen, Z. Bi, C.-F. Tsai, J. Lee, Q. Su, X. Zhang, Q. Jia, J.L. MacManus-Driscoll, H. Wang, Tunable low-field magnetoresistance in (La0.75r0.3Mn03)0.5:(Zn0)0.5 self-assembled vertically aligned nanocomposite thin films, Adv. Funct. Mater. 21 (13) (2011) 2423–2429.
- [30] P. Shekhar, J. Atkinson, Z. Jacob, Hyperbolic metamaterials: fundamentals and applications, Nano Converg. 1 (1) (2014) 14.
- [31] V. Amendola, R. Pilot, M. Frasconi, O.M. Maragò, M.A. Iatì, Surface plasmon resonance in gold nanoparticles: a review, J. Phys. Condens. Matter. Inst. Phys. J. 29 (20) (2017) 203002.